Difference and Linkage in Climate Change Modes from East and Central Asia at Multi-Time Scales

Simin Peng
Lanzhou University
Yu Li (liyu@lzu.edu.cn)
Lanzhou University https://orcid.org/0000-0003-3381-5372

Research Article

Keywords: East Asia (EA), Central Asia (CA), difference and linkage, rain and heat periods, multi-time scales

Posted Date: November 9th, 2021

DOI: https://doi.org/10.21203/rs.3.rs-1048223/v1

Abstract

Previous studies argued that climate change modes from East and Central Asia (EA and CA) are out of phase at multi-time scales. However, in recent years, dry/wet changes in CA which contradict traditional views have provoked further discussion. The synchronization of rain and heat periods is a common climate phenomenon in most regions of East and Central Asia. In this paper, we selected EA and CA to carry out a comprehensive study of modern observations, paleoclimate records, and model simulations at multi-time scales. EOF analysis results of modern grid precipitation and self-calibrating Palmer Drought Severity Index (scPDSI) demonstrate the synchronization of rain and heat periods in EA and the east of CA at the short-term timescale. Meanwhile, paleoclimate records indicate parallel dry/wet changes in EA and the east of CA since the Last Glacial Maximum (LGM), also reflecting the synchronization of rain and heat periods at long-term timescales triggered by the insolation. The climate mechanism of difference and linkage in climate change modes from EA and CA, under the framework of the synchronization of rain and heat periods, is analyzed by PMIP3 simulations between the LGM and Mid-Holocene (MH). Overall, we suggest that, in addition to the regional differences caused by different circulation systems (the westerlies and Asian summer monsoon), climate change modes in EA and CA universally have inter-regional connections affected by the synchronization of rain and heat periods at multi-time scales.

1 Introduction

As typical mid-latitude climatic regions, East and Central Asia (EA and CA) are commonly featured with vigorous circulations and are dominated by the two atmospheric systems, namely mid-latitude westerlies and Asian monsoon (Li, 1990; Zhang and Lin, 1992; Chen et al., 2008; Nagashima et al., 2011). CA, where precipitation is scarce throughout the year, is one of the most arid regions in the mid-latitudes dominated by westerlies (Chen et al., 2009; Huang et al., 2015). Affected by the Asian summer monsoon that carries water vapor from the Ocean, the monsoon-dominated EA has more precipitation (Wang et al., 2017). Over the past few years, there have been many comparative studies of dry/wet changes at multi-time scales from EA and CA. Early works suggested that the climate mode of ‘cold-wet’ or ‘warm-dry’ occurred in northwestern China during the last glacial/interglacial cycle, different from the ‘cold-dry’ or ‘warm-wet’ modes of the monsoon climate (Li, 1990; Han and Qu, 1992; Han et al., 1993). Based on the integration of paleoclimate records, modern meteorological observation data, and paleoclimate simulations, Chen et al. (2008, 2009, 2019) revealed the ‘westerlies-dominated climatic regime’ in arid CA from millennium to interdecadal timescales, which is being out-of-phase or anti-phased with the climate change in the monsoon-dominated region. However, the paleoclimate records of some regions in CA provide asynchronous climate evolution history, in contradiction with the humidity changes caused by the westerlies (An et al., 2006; Zhao et al., 2015; Wang et al., 2018). The latest studies proposed that the persistent weakening of East Asian summer monsoon since 1958, causing an increasing contribution of the monsoonal water vapor transport, thereby enhances summer precipitation in arid CA (Chen et al., 2020; Chen et al., 2021). Therefore, further research is needed to explain dry/wet changes between regions and explore the relationship between climate change modes in EA and CA at multi-time scales.

The synchronization of rain and heat periods is an important phenomenon at the multi-time scale climate change in EA and CA, behaving as that the summer half-year at the short-term timescale and warm period at the long-term timescale has more precipitation than the winter half-year and cold period respectively. In this study, utilizing modern observations, paleoclimate proxies, and model simulations, we conducted a comprehensive analysis for the differences and connections of climate change modes at multi-time scales between EA and CA based on the synchronous phenomenon of rain and heat periods and reasonably explain the "pattern differences" and "spatial connections" between the two regions.

2 Materials And Methods

2.1 Modern observation

The monthly high-resolution (0.5°×0.5°) land precipitation data (referred to as CRU TS4.01) and self-calibrating Palmer Drought Severity Index (referred to as CRU scPDSI 4.05early) are selected from a Climatic Research Unit (CRU) updated gridded climate dataset in the University of East Anglia (van der Schrier et al., 2013; Harris et al., 2014; Barichivich et al., 2021). The CRU monthly climate archives obtain from the auspices of the World Meteorological Organization (WMO) in league with the US National Oceanographic and Atmospheric Administration (NOAA, via its National Climatic Data Center, NCDC).

Empirical orthogonal function (EOF) is a powerful method for dimensionality reduction and pattern extraction. EOF can decompose the multidimensional climate data from different locations into spatial (EOF modes) and temporal functions (principal components). Therefore, to investigate the spatiotemporal variations of precipitation at the interannual timescale over EA and CA, the EOF analysis was applied to the gridded precipitation data and scPDSI. We focused on the first two leading modes that objectively account for the majority of dry/wet changes in EA and CA (Lorenz, 1956).

2.2 Regional and global paleoclimatic proxy data

Here we compiled various LGM paleoclimate records to reconstruct long-term climate variability and primarily paid close attention to paleo-precipitation and moisture changes since the LGM. The $\delta^{13}C$, $\delta^{18}O$, TOC, C/N was mainly selected to indicate the climate changes. As all, in this paper we have selected records based on three criteria: (1) the selected records must have a reliable chronology. (2) The record length should cover most of the LGM without documented depositional hiatuses. (3) Proxies should have clear meanings showing dry/wet status. Following the above criteria, we collect typical proxy data from various paleoclimate records in EA and CA (Table 1 and Fig. 1a) since the LGM.

Table 1
Proxies selected in this study to indicate changes in wet/dry status or precipitation.

Section	Lat	Lon	Dating Method	Proxy	References
Hulu Cave	32.500	119.167	U-Th	$\delta^{18}O$	Wang et al., 2001
Dongge Cave	25.283	108.083	U-Th	$\delta^{18}O$	Dykoski et al., 2005
Kesang Cave	42.867	81.750	U-Th	$\delta^{18}O$	Cheng et al., 2016a, 2016b
Qinghai Lake	37.000	100.000	^{14}C	$\delta^{18}O$	Liu et al., 2007
Lake Karakul	39.018	73.533	^{14}C	$\delta^{13}C$	Heinecke et al., 2017
Ulaan Nuur	44.530	103.630	OSL	TOC	Lee et al., 2013
Xinjiang loess	43.970	85.330	^{14}C	MS	Chen et al., 2016
Achit Nuur	49.417	90.517	^{14}C	$\delta^{18}O$	Sun et al., 2013
Caspian Sea	37.170	54.060	^{14}C	$\delta^{18}O$	Leroy et al., 2014
Balikun Lake	43.670	92.800	^{14}C	pollen	Zhao et al., 2015

2.3 Paleoclimatic simulations

The Paleoclimate Modeling Intercomparison Project (PMIP) was launched to coordinate and encourage the systematic study of General Circulation Models (GCMs) and to understand the mechanisms of climate change and the role of climate feedbacks (Joussaume et al., 1999) (Table 2). Eight coupled GCMs covering the LGM or MH from the PMIP3 database were selected to analyze the mechanisms of climate change in this study (Table 3). The output data of the PMIP3 in the LGM and MH are available at htQTPs://esgf-node.llnl.gov/search/esgf-llnl/. By chiefly interpolating various climate variables on the common 1°×1° grid and then sorting the values of model simulations from minimum to maximum, we extracted the median value of all PMIP3 models used in this paper to evaluate the PMIP3 model simulations and acquire the scientific model simulation value.

Table 2
Boundary conditions and forcing for PMIP3-CMIP5 models at the LGM and MH.

Period	Eccentricity	Obliquity (°)	Longitude of perihelion (°)	CO_2 (ppm)	CH_4 (ppb)	N_2O (ppb)	Ice sheet	Vegetation
LGM	0.018994	22.949	114.425	185	350	200	Peltier (2004), 21 ka	Present day
MH	0.018682	24.105	0.87	280	650	270	Peltier (2004), 0 ka	Present day

Table 3
Basic information about climate models from PMIP3-CMIP5 used in this study.

Model	Institute	Resolutions	Variables*	References
bcc-csm1-1	Beijing Climate Center, China Meteorological Administration, China	64×128 (17)	ua, va, zg, hus, psl, pr, tas	Randall et al. (2007)
CNRM-CM5	Centre National de Recherches Météorologiques, France	128×256 (17)	ua, va, zg, hus, psl, pr, tas	Voldoire et al. (2013)
CCSM4	National Center for Atmospheric Research, USA	288×192 (17)	ua, va, zg, hus, psl, pr, tas	Gent et al. (2011)
CSIRO-Mk3-6-0	Australian Commonwealth Scientific and Industrial Research Organization Marine and Atmospheric Research in collaboration with the Queensland Climate Change Centre of Excellence, Australia	96×192 (18)	ua, va, zg, hus, psl, pr, tas	Rotstayn et al. (2010)
GISS-E2-R	NASA Goddard Institute for Space Studies, USA	144×90 (17)	ua, va, zg, hus, psl, pr, tas	Schmidt et al. (2014)
MIROC-ESM	Japan Agency for Marine-Earth Science and Technology, Japan	128×64 (35)	ua, va, zg, hus, psl, pr, tas	Watanabe et al. (2011)
FGOALS-s2	LASG-CEES. China	108×128 (17)	ua, va, zg, hus, psl, pr, tas	Briegleb et a1. (2004)
MRI-CGCM3	Meteorological Research Institute, Japan	320×160 (23)	ua, va, zg, hus, psl, pr, tas	Yukimoto et al. (2012)

*: ua means eastward_wind; va means northward wind; zg geopotential Height; hus near-surface relative humidity; psl means sea surface pressure; pr means precipitation; tas means near-surface temperature

3. Results And Discussion

3.1 Synchronization of rain and heat periods at the short-term timescale

We calculated the precipitation difference between the summer (April, May, June, July, August, and September) and winter (January, February, March, October, November, and December) half year over 1965-2014, and then defined the region greater than 0 mm as the synchronous region of rain and heat periods (Fig. 1, gray slash). The East Asian summer monsoon boundary was depicted by the seasonality in precipitation according to the definition of the summer monsoon index by Wang et al. (2012) (Fig. 1,

red line). Based on this, we defined the monsoon region as EA, and the non-monsoon region as CA, in particular, the asynchronous region of rain and heat periods is the core region of CA (Fig. 1). It can be seen that the synchronous region of rain and heat periods covers most of the non-monsoon region (i.e., the east of CA). To obtain the spatial distribution characteristics of the precipitation and scPDSI anomalies in EA and CA under the context of synchronization of rain and heat periods, we conducted an EOF analysis on the precipitation and scPDSI standardized anomaly field over 1965-2014.

Figure 2a-d shows the spatial distribution and time series of EOF decomposition of mean annual precipitation. The variance contribution rate of the first mode is 9.55%, showing an obvious dipole mode. The center of positive values is in the CA core mainly belonged to the asynchronous region of rain and heat periods, while the center of negative values is in the south of EA located in the synchronous region of rain and heat periods (Fig. 2a). The opposite signals indicate that the mean annual precipitation changes in the asynchronous and synchronous regions show a see-saw pattern. The first mode exhibits the interdecadal and interannual changes according to the PC1 (Fig. 2b). The variance contribution rate of the second mode is 9.08%, indicating zonal dipole distribution characteristics (Fig. 2c). The center of positive values is in the north of CA, and the center of negative values is in the east of CA and northeast of EA, displaying the spatial diversity of climate change in the synchronous region of rain and heat periods (Fig. 2c). The PC2 shows that the second mode has significant interdecadal characteristics (Fig. 2d). Alternatively, we analyzed the spatial distribution and time series of EOF decomposition of precipitation difference between summer and winter half-year (Fig. 1e-h). The variance contribution rate of the first mode is 10.47%, which is a meridional bipolar distribution (Fig. 2e). The center of the negative value is located in the north of EA and CA, according with the synchronization of rain and heat periods in the non-monsoon region. The variance contribution rate of the second mode is 8.35%, displaying a dipole mode (Fig. 2e). The positive load in EA illustrates the effect of the synchronization of rain and heat periods (Fig. 2e). Simultaneously, the PC1 and PC2 exhibit that in contrast to mean annual precipitation, the amplitude of dry/wet changes and the characteristics of interannual changes in EA and CA are more prominent (Fig. 2f and h).

The variance contribution rate of the first mode of mean annual scPDSI is 13.58%, showing an obvious dipole mode (Fig. 3a). The centers of positive values are mainly distributed in the core and northern part of CA, while the negative values are mainly distributed in EA and the east of CA (Fig. 3a). This spatial distribution also shows that EA and the east of CA, both of which belong to the synchronous region of rain and heat periods, have the same dry/wet status, in contrast to the core and northern part of CA. The first mode exhibits the interdecadal changes according to the PC1 (Fig. 3b). The variance contribution rate of the second mode is 11.58% (Fig. 2c), with the center of positive values in EA and the east of CA. The PC2 shows that the second mode has significant interdecadal characteristics opposite to the mean annual precipitation (Fig. 3d and 2d). The variance contribution rate of the first mode of scPDSI difference between summer and winter half-year is 8.63%, which is a bipolar distribution (Fig. 2e). The center of the positive value is located in the north of EA and northeast of CA, indicating the generally consistent dry/wet change in the synchronous region of rain and heat periods, which is different from the core region of CA. The variance contribution rate of the second mode is 8.35%, displaying a zonal dipole

mode between the synchronous region of rain and heat periods and the core region of CA (Fig. 2e). The PC1 and PC2 of scPDSI difference between summer and winter half-year the intense amplitude of dry/wet changes and interannual changes (Fig. 3f and h).

In all, the spatial distribution and time series of EOF decomposition of mean annual scPDSI are significantly similar to that of precipitation, collectively indicated that EA and the east of CA, which belong to the synchronous region of rain and heat periods, have similar dry/wet changes. Therefore, we suggest that synchronization of rain and heat periods is an important factor linking climate change mode in EA and CA at the short-term timescales.

3.2 Synchronization of rain and heat periods at the long-term timescales

In the last decade, several paleoclimate records with a relatively high resolution, reliable chronology, and unambiguous proxies have been published to discuss the long-term timescale climate evolution in EA and CA. According to the model simulation, Yu et al. (2000) concluded that the low temperature in the cold period causes the decreasing evaporation, with the enhanced westerlies driven by expanding land ice sheets, forming the high lake level in western China and the low lake level in eastern China during the LGM. The reconstructed precipitation covering the past 22,600 years from Achit Nuur suggests the wet periods from 22,600 to 13,200 cal BP (Sun et al., 2013) (Fig. 4h). In the Holocene, pollen record of the Caspian Sea displays that the terrestrial vegetation around the Caspian Sea changed from desert and desert steppe during the last glacial to dry shrubland and forest from the early-Holocene to late-Holocene, revealing the continuous wetting process since the early Holocene and the wettest late-Holocene (Leroy et al., 2013) (Fig. 4j). Meanwhile, results of climatically-sensitive magnetic properties from the Xinjiang loess demonstrate that the relatively moist conditions are generally formed after ~6,000 cal BP, with the wettest climate occurring during the late Holocene, and that a dry climate prevailed during the early Holocene (Chen et al., 2016) (Fig. 4i). To sum up, most views believed that the climate change mode in CA (non-monsoon region) affected by the westerlies, characterized by wet climate conditions during the LGM and mid- and late-Holocene (Fig. h-j), is opposite to that in monsoon-dominated EA (Fig. 4b).

However, there are still partially contradictory long-term timescales dry/wet changes in CA, which are different from the climate change mode in CA but similar to that in EA. Herzschuh. (2006) comprehensively analyzed 75 paleoclimatic records in CA and revealed that wet conditions occurred during early- and mid-Holocene, while the LGM was characterized by dry climate conditions in the region (Fig. 4c), indicating the similarity with monsoon climate represented by the speleothem $\delta^{18}O$ records from Dongge Cave and Hulu Cave (Fig. 4b). High precipitation observed between early- and mid-Holocene, indicated by $\delta^{18}O$ records of ostracod shells from Qinghai Lake, shows that the climate in Qinghai Lake since the late Glacial reflects the monsoon change (Liu et al, 2007) (Fig. 4e). The climate in Ulaan Nuur was most humid during the early Holocene, humid during the mid-Holocene and dry in the late-Holocene, embodying a typical characteristic of the East Asian monsoon (Lee et al., 2013) (Fig. 4f). Based on a sediment core from Lake Karakul, the early- to mid-Holocene is characterized by moister conditions in the

region, and the lake level remained low during the LGM (Heinecke et al., 2017) (Fig. 4d). Furthermore, the regional climate in western China, inferred from speleothem oxygen-carbon isotope in Kesang Cave, suggests a close coupling with the Asian summer monsoon (Cheng et al., 2016) (Fig. 4g). The lake level and climate reconstructed results also suggested that the cold-dry LGM climate triggered a substantial lowering of lake level in most of arid western China, challenging the traditional view of cold-wet climate and high lake levels in arid western China during the LGM (Zhao et al., 2015).

Considering the spatial distribution of the above paleoclimate records, we found that the Central Asian records similar to the monsoon evolution are located in the modern synchronous region of rain and heat periods (Fig. 1a). At the same time, the dry climate condition during the LGM and the wet climate change mode during the early- and mid-Holocene also reflect another meaning of the synchronization of rain and heat periods at long-term timescales triggered by the insolation (Fig. 4a), namely the dry-cold period and wet-warm period.

3.3 Climate mechanism of difference and linkage in climate change modes from EA and CA at the long-term timescale

The results of paleoclimate simulations explain the asynchrony of the long-term climate change mode in EA and CA and the climate linkages under the framework of the synchronization of rain and heat periods at the long-term timescale. During the LGM, lower summer insolation increases the meridional difference of temperature and sea level pressure in the summer half-year (rain period) large (Fig. 4a; 5a-b), leading to the strengthening of the westerly jet stream and further increasing the precipitation in the core region of CA (Fig. 5c and h). Given the weakening of the LGM summer monsoon and the complex control factors (Fig. 5g), however, the precipitation in the east of CA is weaker than that of MH (Fig. 5c), which is consistent with the climate change mode in EA and reflects climate linkage between CA and EA caused by synchronization of rain and heat periods. Although the westerly jet stream weakens in the LGM winter half-year (Fig. 5i), the higher winter insolation contributes to the general warming in CA and EA (Fig. 4a; 5d), resulting in lower relative humidity (Fig. 5e). According to climatological theory (Barry and Richard, 2009), a decrease in relative humidity means an increase in saturated water vapor pressure, which ultimately leads to an increase in precipitation (Fig. 5f). Therefore, this elaborates the asynchrony of the long-term climate change mode in EA and CA under the background of synchronization of rain and heat periods.

4. Conclusion

Using EOF method, this study analyzes the spatiotemporal variations of precipitation and short-term scPDSI in EA and CA. Results reveal that the synchronization of rain and heat periods is an important factor linking climate change modes in EA and CA at short-term timescales. Concurrently, paleoclimate records reflect the synchronization of rain and heat periods at long-term timescales triggered by the insolation. The model simulations of multiple climatic elements explain the climate mechanism of differences and linkages in climate change modes from EA and CA. In the context of asynchronous

dry/wet changes between monsoon- and the westerlies-dominated regions, we believe that regional linkages also exist in EA and CA.

Declarations

Acknowledgement

This research was supported by the National Natural Science Foundation of China (Grant No. 42077415, 41822708); the National Key Research and Development Program of China (No. 2019YFC0507401); the Second Tibetan Plateau Scientific Expedition and Research Program (STEP) (Grant No. 2019QZKK0202); the Strategic Priority Research Program of Chinese Academy of Sciences (Grant No. XDA20100102); the 111 Project (BP0618001).

Conflicts of interest/Competing interests

The authors declare no competing financial interests.

References

1. An, C.B., Feng, Z.D., & Barton, L. (2006). Dry or humid? Mid-Holocene humidity changes in arid and semi-arid China. Quat. Sci. Rev. 25(3-4): 351-61.
2. Barichivich, J., Osborn, T.J., Harris, I., van der Schrier, G., & Jones, P.D. (2021). Monitoring global drought using the self-calibrating Palmer Drought Severity Index [in \State of the Climate in 2020\]. Bulletin of the American Meteorological Society xx, Sxx-Sxx.
3. Barry, R.G. & Richard, J.C. (2009). Atmosphere, weather and climate. Routledge.
4. Briegleb, B.P., Bitz, C.M., Hunke, E.C., Lioscomb, W.H., Holland, M.M., Schramm, J.L., et al. (2004). Scientific description of the sea ice component in the community climate system model, version three.
5. Chen, C., Zhang, X., Lu, H., Jin, L., Du, Y., Chen, F. (2021a). Increasing summer precipitation in arid central Asia linked to the weakening of the East Asian summer monsoon in the recent decades. Int J Climatol, 41: 1024-1038
6. Chen, F., Chen, J., Huang, W. (2021b). Weakened East Asian summer monsoon triggers increased precipitation in Northwest China. Sci. China-Earth Sci, 64(5): 835-837, https://doi.org/10.1007/s11430-020-9731-7
7. Chen, F., Chen, J., Huang, W., Chen, S., Huang, X., Jin, L., Jia, J., Zhang, X., An, C., Zhang, J., Zhao, Y. (2019). Westerlies Asia and monsoonal Asia: spatiotemporal differences in climate change and possible mechanisms on decadal to suborbital timescales. Earth-Sci. Rev. 192, 337–354.
8. Chen, F., Jia, J., Chen, J., Li, G., Zhang, X., Xie, H., ... & An, C. (2016). A persistent Holocene wetting trend in arid central Asia, with wettest conditions in the late Holocene, revealed by multi-proxy analyses of loess-paleosol sequences in Xinjiang, China. Quat. Sci. Rev., 146, 134-146.

9. Chen, F.H., Chen, J.H., Huang, W. (2009). A discussion on the westerly-dominated climate model in mid-latitude Asia during the modern interglacial period. Earth Sci. Front. 16, 23-32 (in Chinese with English abstract).
10. Chen, F.H., Yu, Z.C., Yang, M.L., Ito, E., Wang, S.M., David, B.M., Huang, X.Z., Zhao, Y., Sato, T., Birks, H.J.B., Boomer, I., Chen, J.H., An, C.B., Wünnemann, B. (2008). Holocene moisture evolution in arid Central Asia and its out-of-phase relationship with Asian monsoon history. Quat. Sci. Rev. 27, 351–364.
11. Cheng, H., Edwards, R.L., Sinha, A., Spötl, C., Yi, L., Chen, S., Kelly, M., Kathayat, G., Wang, X., Li, X., Kong, X. (2016a). The Asian monsoon over the past 640000 years and ice age terminations. Nature 534, 640–646.
12. Cheng, H., Spötl, C., Breitenbach, S.F., Sinha, A., Wassenburg, J.A., Jochum, K.P., Scholz, D., Li, X., Yi, L., Peng, Y., Lv, Y. (2016b). Climate variations of central Asia on orbital to millennial timescales. Sci. Rep. 5, 36975. https://doi .org /10 .1038 / srep36975.
13. Dykoski, C.A., Edwards, R.L., Cheng, H., Yuan, D., Cai, Y., Zhang, M., Lin, Y., Qing, J., An, Z., Revenaugh, J. (2005). A high-resolution, absolute-dated Holocene and deglacial Asian monsoon record from Dongge Cave, China. Earth Planet. Sci. Lett. 233, 71–86.
14. Gent, P.R., Danabasoglu, G., Donner, L.J., Holland, M.M., Hunke, E.C., Jayne, S.R., Lawrence, D.M., Neale, R.B., Rasch, P.J., & Vertenstein, M. (2011). The community climate system model version 4, J. Climate., 24, 4973-4991, https://doi.org/10.1175/2011JCLI4083.1.
15. Han, S.T., Qu, Z. (1992). Inland Holocene climatic features recorded in Balikun lake, northern Xinjiang. Sci. China Ser. B 11, 1201-1209 (in Chinese).
16. Han, S.T., Wu, N.Q., Li, Z.Z. (1993). Inland climate changes in Dzungaria during the late Pleistocene Epoch. Geogr. Res. 12, 47-54 (in Chinese with English abstract).
17. Harris, I., Jones, P.D., Osborn, T.J., Lister, D.H. (2014). Updated high-resolution grids of monthly climatic observations-the CRU TS3.10 Dataset. Int. J. Climatol. 34 (3), 623-642. https://doi.org/10.1002/joc.3711.
18. Heinecke, L., Mischke, S., Adler, K., Barth, A., Biskaborn, B. K., Plessen, B., ... & Herzschuh, U. (2017). Climatic and limnological changes at Lake Karakul (Tajikistan) during the last~ 29 cal ka. J. Paleolimnology, 58(3), 317-334.
19. Herzschuh, U. (2006). Palaeo-moisture evolution in monsoonal central Asia during the last 50,000 years. Quat. Sci. Rev. 25(1-2), 163-178.
20. Huang, W., Chen, J.H., Zhang, X.J., Feng, S., Chen, F.H. (2015). Definition of the core zone of the “westerlies-dominated climatic regime”, and its controlling factors during the instrumental period. Sci. China Earth Sci. 58, 676-684.
21. Joussaume, S., Taylor, K.E., Braconnot, P.J.F.B., Mitchell, J.F.B., Kutzbach, J.E., Harrison, S.P., Prentice, I.C., Broccoli, A.J., Abe-Ouchi, A., Bartlein, P.J., Bonfils, C. (1999). Monsoon changes for 6000 years ago: results of 18 simulations from the paleoclimate modeling intercomparison project (PMIP). Geophys. Res. Lett. 26, 859-862.

22. Lee, M.K., Lee, Y.I., Lim, H.S., Lee, J.I., & Yoon, H.I. (2013). Late Pleistocene-H olocene records from Lake Ulaan, southern Mongolia: implications for east Asian palaeomonsoonal climate changes. J. Quat. Sci. 28(4), 370-378.
23. Leroy, S.A., López-Merino, L., Tudryn, A., Chalié, F., & Gasse, F. (2014). Late Pleistocene and Holocene palaeoenvironments in and around the middle Caspian basin as reconstructed from a deep-sea core. Quat. Sci. Rev. 101, 91-110.
24. Li, J.J. (1990). The patterns of environmental changes since last Pleistoc ene in northwestern China. Quat. Sci. 3, 197-204 (in Chinese with English abstract).
25. Liu, X.Q., Shen, J., Wang, S.M., Wang, Y.B., Liu, W.G. (2007). Southwest monsoon changes indicated by oxygen isotope of ostracode shells from sediments in Qinghai lake since the late glacial. Chin. Sci. Bull. 4, 109-114.
26. Lorenz, E.N. (1956). Empirical orthogonal function and statistical weather prediction. Scientific Report No. 1 Statist Forecasting Project. Department of Meteorology, Massachusetts Institute of Technology.
27. Nagashima, K., Tada, R., Tani, A., et al. (2011). Millennial-scale oscillations of the westerly jet path during the last glacial period. Journal of Asian Earth Sciences, 40 1214-1220.
28. Peltier, W.R. (2004). Global glacial isostasy and the surface of the ice-age Earth: The ICE-5G (VM2) model and GRACE, Annu. Rev. Earth Pl. Sc., 32, 111-149, https://doi.org/10.1146/annurev.earth.32.082503.144359.
29. Randall, D.A., Wood, R.A., Bony, S., Colman, R., & Taylor, K.E. (2007). Climate models and their evaluation. Cambridge University Press.
30. Rotstayn, L., Collier, M., Dix, M., Feng, Y., Gordon, H., O\\\'Farrell, S., Smith, I. and Syktus, J. (2010). Improved simulation of Australian climate and ENSO-related climate variability in a GCM with an interactive aerosol treatment. Int. J. Climatology, vol 30(7), pp1067-1088,
31. Schmidt, G.A., Kelley, M., Nazarenko, L., Ruedy, R., Russell, G. L., Aleinov, I., Bauer, M., Bauer, S. E., Bhat, M. K., Bleck, R., Canuto, V., Chen, Y. H., Cheng, Y., Clune, T. L., Genio, A. D., de Fainchtein, R., Faluvegi, G., Hansen, J. E., Healy, R. J., Kiang, N. Y., Koch, D., Lacis, A. A., LeGrande, A. N., Lerner, J., Lo, K. K., Matthews, E. E., Menon, S., Miller, R. L., Oinas, V., Oloso, A. O., Perlwitz, J. P., Puma, M. J., Putman, W. M., Rind, D., Romanou, A., Sato, M., Shindell, D. T., Sun, S., Syed, R. A., Tausnev, N., Tsigaridis, K., Unger, N., Voulgarakis, A., Yao, M. S., & Zhang, J. L. (2014). Configuration and assessment of the GISS ModelE2 contributions to the CMIP5 archive. J. Adv. Model. Earth Sy., 6, 141–184, https://doi.org/10.1002/2013ms000265.
32. Sun, A., Feng, Z., Ran, M., & Zhang, C. (2013). Pollen-recorded bioclimatic variations of the last~ 22,600 years retrieved from Achit Nuur core in the western Mongolian Plateau. Quat. Int. 311, 36-43.
33. van der Schrier, G., Barichivich, J., Briffa, K.R., et al. (2013). A scPDSI-based global data set of dry and wet spells for 1901–2009. J. Geophys. Res.-Atmos. 118(10): 4025-4048.

34. Voldoire, A., Sanchez-Gomez, E., Mélia, D. S. Y., Decharme, B., Cassou, C., Sénési, S., et al. (2013). The CNRM-CM5.1 global climate model: Description and basic evaluation. Clim. Dyn. 40, 2091-2121. https://doi.org/10.1007/s00382-011-1259-y.
35. Wang, L., Jia, J., Xia, D., et al. (2018). Climate change in arid central Asia since MIS 2 revealed from a loess sequence in Yili Basin, Xinjiang, China. Quat. Int. S1040618217315379.
36. Wang, B., Liu, J., Kim, H. J., Webster, P. J., & Yim, S. Y. (2012). Recent change of the global monsoon precipitation (1979–2008). Clim. Dyn. 39(5), 1123-1135.
37. Wang, P.X., Wang, B., Cheng, H., Fasullo, J., Guo, Z., Kiefer, T., & Liu, Z. (2017). The global monsoon across time scales: Mechanisms and outstanding issues. Earth Sci. Rev. 174, 84-121.
38. Wang, Y.J., Cheng, H., Edwards, R.L., An, Z.S., Wu, J.Y., Shen, C.C., & Dorale, J.A. (2001). A high-resolution absolute-dated late Pleistocene monsoon record from Hulu cave, China. Science 294 (5550), 2345–2348. https://doi .org /10 .1126 /science .1064618.
39. Watanabe, S., Hajima, T., Sudo, K., Nagashima, T., Takemura, T., Okajima, H., Nozawa, T., Kawase, H., Abe, M., Yokohata, T., Ise, T., Sato, H., Kato, E., Takata, K., Emori, S., and Kawamiya, M. (2011). MIROC-ESM 2010: model description and basic results of CMIP5-20c3m experiments, Geosci. Model Dev., 4, 845–872, https://doi.org/10.5194/gmd-4-845-2011, 2011.
40. Yu, G., Xue, B., Wang, S.M., et al. (2000). Chinese lakes records and the climate significance during Last Glacial Maximum. Chinese Science Bulletin, 45(3): 250-255 (in Chinese with English abstract).
41. Yukimoto, S., Adachi, Y., Hosaka, M., Sakami, T., Yoshimura, H., Hirabara, M., Tanaka, T. Y., Shindo, E., Tsujino, H., & Deushi, M. (2012). A new global climate model of the Meteorological Research Institute: MRI-CGCM3: Model description and basic performance, J. Meteorol. Soc. Jpn., 90, 23–64, https://doi.org/10.2151/jmsj.2012-a02.
42. Zhang, J.C. & Lin, Z.G. (1992). Climate of China. Wiley, New York.
43. Zhang, J., Nottebaum, V., Tsukamoto, S., Lehmkuhl, F., & Frechen, M. (2015). Late Pleistocene and Holocene loess sedimentation in central and western Qilian Shan (China) revealed by OSL dating. Quat. Int. 372, 120-129.
44. Zhao, Y., An, C., Mao, L., Zhao, J., Tang, L., Zhou, A., Li, H., Dong, W., Duan, F., & Chen, F. (2015). Vegetation and climate history in arid western China during MIS2: New insights from pollen and grain-size data of the Balikun Lake, eastern Tien Shan. Quat. Sci. Rev. 126, 112-125.

Figures

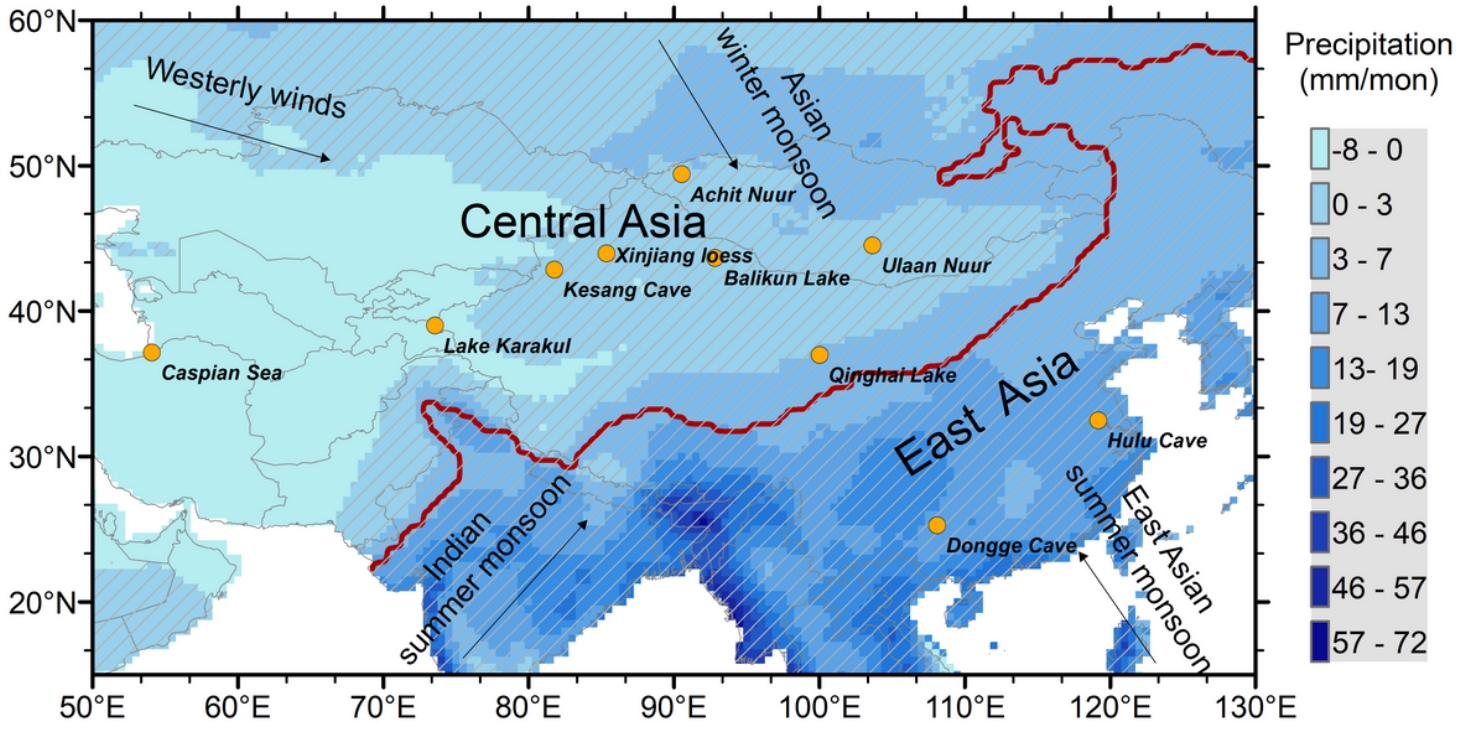

Figure 1

The difference between summer and winter precipitation over 1965-2014 (shade), and the major trajectories of atmospheric circulation. The gray slash represents the synchronous region of the rain and heat periods, the red line represents the locations of the climatological summer monsoon boundary over 1965–2014 (method from wang et al. (2012)), black dots represent the paleoclimate records used in this study.

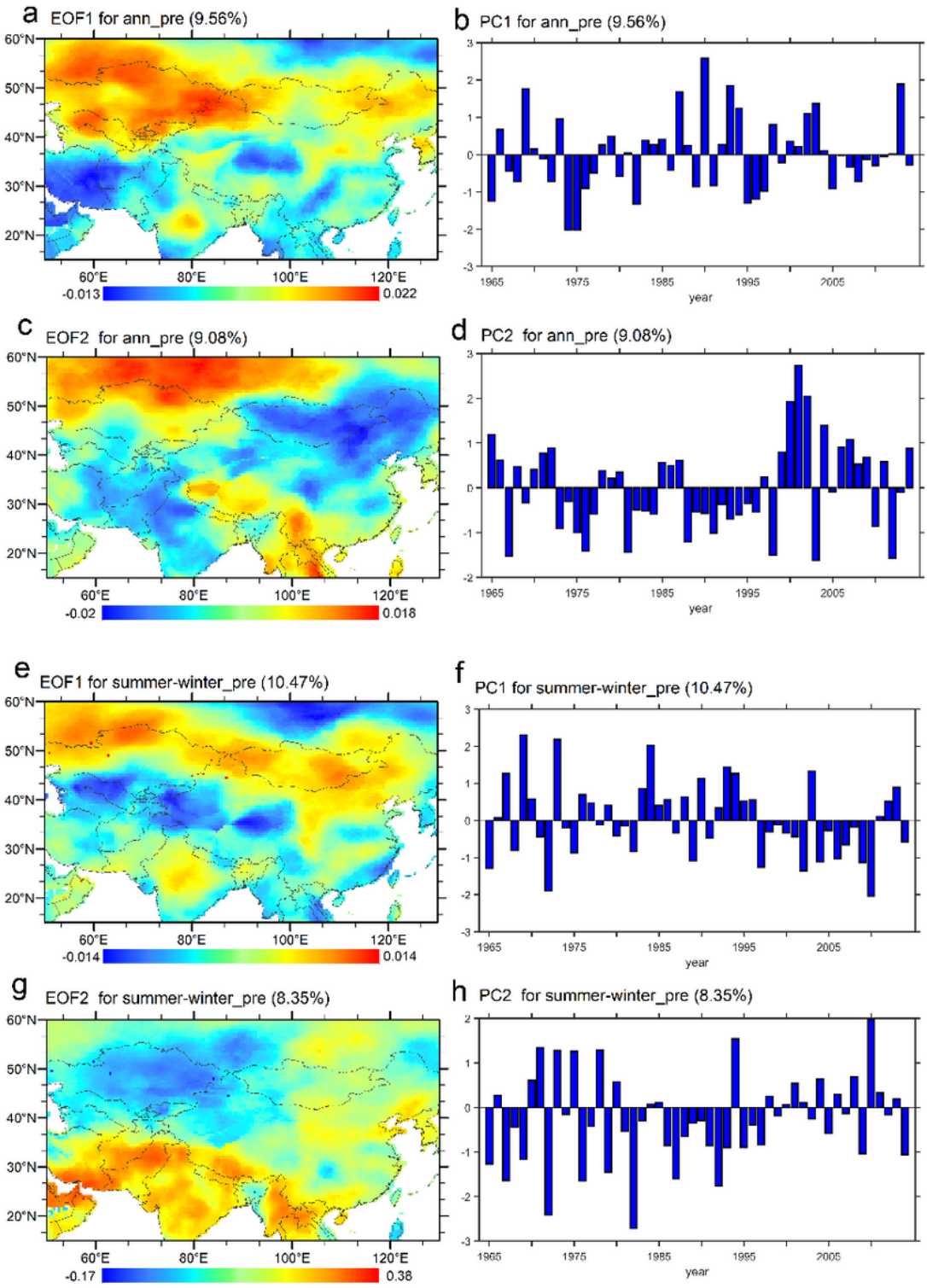

Figure 2

a-d, the EOF modes and corresponding time series of annual mean precipitation in EA and CA over 1965-2014; e-h, the EOF modes and corresponding time series of precipitation difference between summer and winter in EA and CA over 1965-2014.

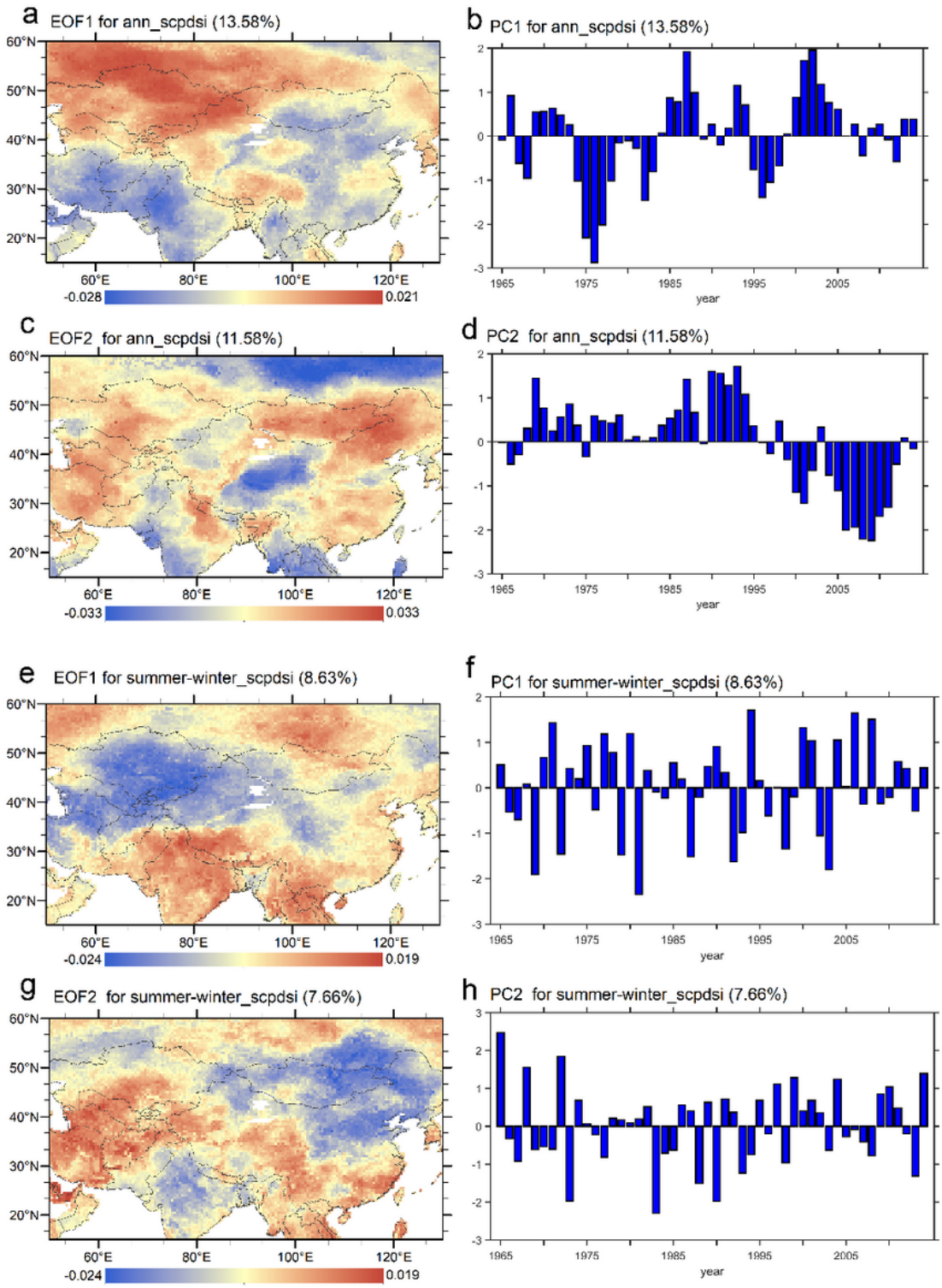

Figure 3

a-d, the EOF modes and corresponding time series of annual mean scPDSI in EA and CA over 1965-2014; e-h, the EOF modes and corresponding time series of scPDSI difference between summer and winter in EA and CA over 1965-2014.

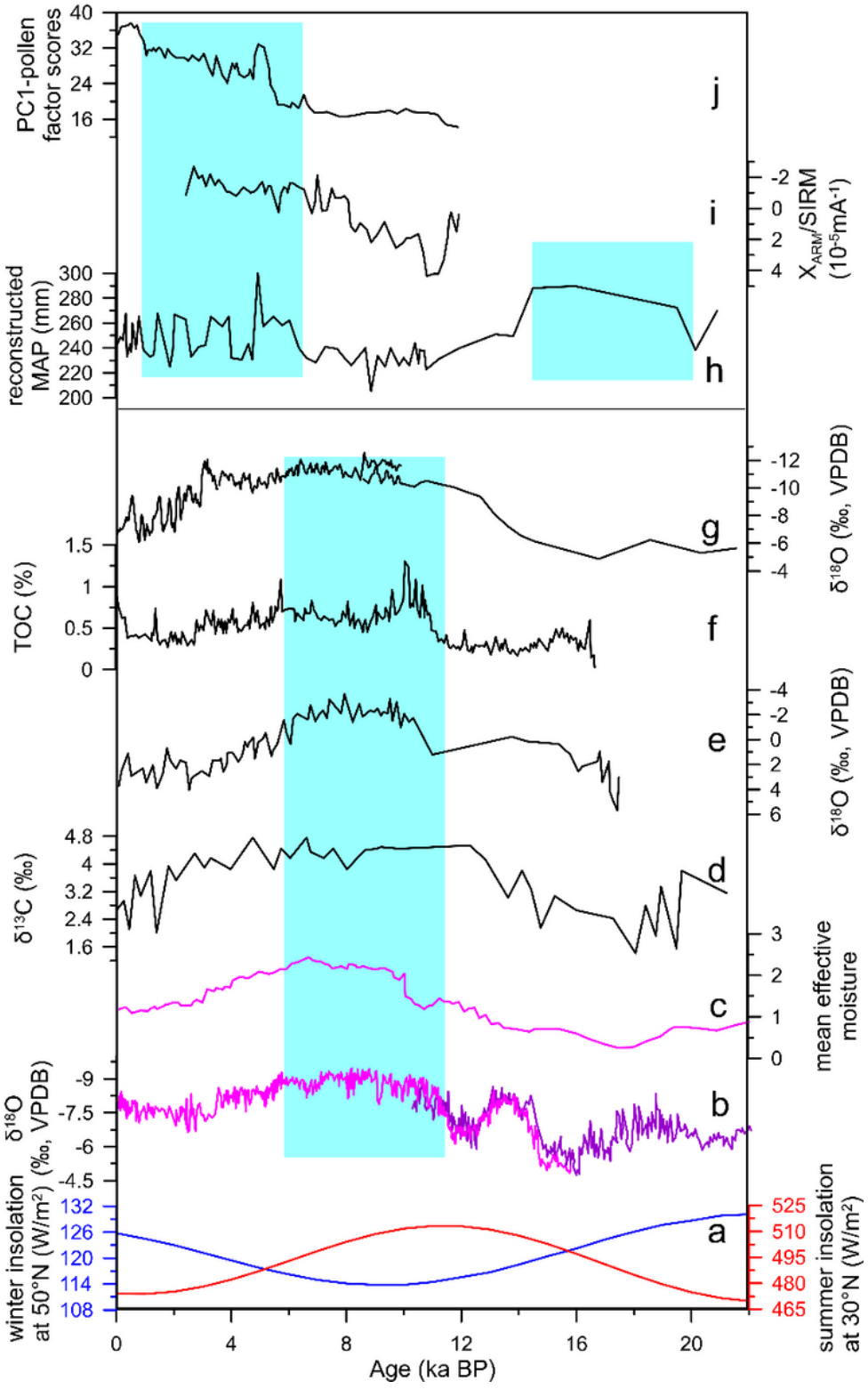

Figure 4

A comparison of proxy variability recorded in EA and CA. a Summer (red line) insolation at 30°N and winter (blue line) insolation at 50°N (Berger, 1978); b Cave speleothem δ18O values records from Dongge Cave and Hulu Cave (Yuan et al., 2004; Wang et al., 2001); c Mean effective moisture from monsoonal Central Asia (Herzschuh, 2006); d δ13C from Lake Karakul (Heinecke et al., 2017); e δ18O of ostracode shells from Qinghai Lake (Liu et al., 2007); f TOC (Total organic carbon) from Ulaan Nuur (Lee et al.,

2013); g δ18O from Kesang Cave (Cheng et al., 2016); h Reconstructed MAP (mean annual precipitation) from Achit Nuur (Sun et al., 2013); i XARM/SIRM in the LJW10 section of the Xinjiang Loess (Chen et al., 2016); j Pollen record from the Caspian Sea (Leroy et al., 2014).

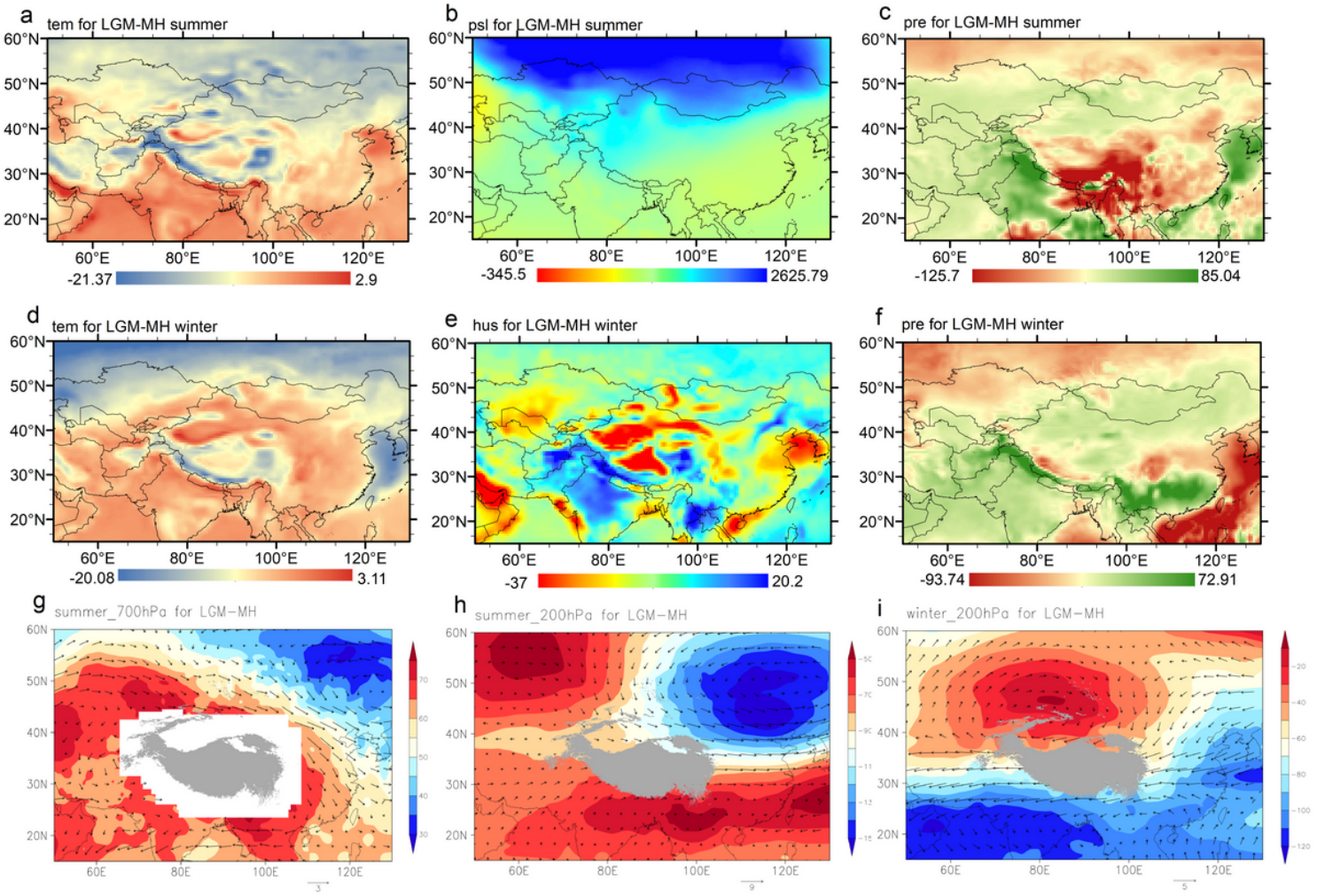

Figure 5

Summer half-year differences of temperature (tem) (a), sea level pressure (psl) (c), precipitation (pre) (e), 700 hPa wind field (g), and 200 hPa wind field (h) for LGM-MH; and winter half-year differences of temperature (b), relatively humid (hus) (d), precipitation (f), and 200 hPa wind field (i) for LGM-MH in EA and CA based on the PMIP3-CMIP5 multi-model ensemble.